

UC Davis

UC Davis Previously Published Works

Title

Soluble epoxide hydrolase-targeting PROTAC activates AMPK and inhibits endoplasmic reticulum stress

Permalink

<https://escholarship.org/uc/item/2z10z7t6>

Authors

Peyman, Mona

Barroso, Emma

Turcu, Andreea L

et al.

Publication Date

2023-12-01

DOI

10.1016/j.biopha.2023.115667

Peer reviewed



Published in final edited form as:

Biomed Pharmacother. 2023 December ; 168: 115667. doi:10.1016/j.biopha.2023.115667.

Soluble epoxide hydrolase-targeting PROTAC activates AMPK and inhibits endoplasmic reticulum stress

Mona Peyman^{1,2,3,4,*}, **Emma Barroso**^{1,2,3,4,*}, **Andreea L. Turcu**^{2,5}, **Francesc Estrany Jr.**^{1,2,3,4}, **Dáire Smith**^{1,2,3,4}, **Javier Jurado-Aguilar**^{1,2,3,4}, **Patricia Rada**^{3,6}, **Christophe Morisseau**⁷, **Bruce D. Hammock**⁷, **Ángela M. Valverde**^{3,6}, **Xavier Palomer**^{1,2,3,4}, **Carles Galdeano**^{2,8}, **Santiago Vázquez**^{2,5}, **Manuel Vázquez-Carrera**^{1,2,3,4}

¹Department of Pharmacology, Toxicology and Therapeutic Chemistry, Faculty of Pharmacy and Food Sciences

²Institute of Biomedicine of the University of Barcelona (IBUB), University of Barcelona, 08028 Barcelona, Spain

³Spanish Biomedical Research Center in Diabetes and Associated Metabolic Diseases (CIBERDEM)-Instituto de Salud Carlos III, 28029 Madrid, Spain

⁴Pediatric Research Institute-Hospital Sant Joan de Déu, 08950 Esplugues de Llobregat

⁵Laboratori de Química Farmacèutica (Unitat Associada al CSIC), Facultat de Farmàcia i Ciències de l'Alimentació, Universitat de Barcelona, Av. Joan XXIII, 27-31, 08028, Barcelona, Spain

⁶Instituto de Investigaciones Biomédicas Alberto Sols (CSIC/UAM), Madrid, Spain

⁷Department of Entomology and Nematology, and UC Davis Comprehensive Cancer Center, University of California, Davis, Davis, California 95616, United States

⁸Department of Pharmacy and Pharmaceutical Technology and Physical Chemistry, Faculty of Pharmacy and Food Sciences, University of Barcelona, 08028 Barcelona, Spain.

Abstract

Soluble epoxide hydrolase (sEH) is a drug target with the potential for therapeutic utility in the areas of inflammation, neurodegenerative disease, chronic pain, and diabetes, among others. Proteolysis-targeting chimeras (PROTACs) molecules offer new opportunities for targeting sEH, due to its capacity to induce its degradation. Here, we describe that the new ALT-PG2, a PROTAC that degrades sEH protein in the human hepatic Huh-7 cell line, in isolated mouse

Corresponding author: Manuel Vázquez-Carrera, Unitat de Farmacologia, Facultat de Farmàcia i Ciències de l'Alimentació, Av. Joan XXIII 27-31, E-08028 Barcelona, Spain. Telephone: (+34) 93 4024531. Fax: (+34) 93 4035982, mvazquezcarrera@ub.edu.

*Both authors contributed equally.

CRedit authorship contribution statement

MP, EB, FE, DS, JJ, PR, CM, BH, AMV, and MVC performed the experiments; ALT and SV conducted the synthesis of the compounds, EB, ALT, XP, CM, BH, CG, SV and MVC analyzed the data, reviewed the results and wrote the manuscript; EB, CG, SV and MVC designed the experiments. MVC is the guarantor of this work and, as such, had full access to all of the data in the study and takes responsibility for the integrity of the data and the accuracy of the data analysis.

Declaration of Competing Interest

The authors have no conflicts of interest to declare.

primary hepatocytes, and in the liver of mice. Remarkably, sEH degradation caused by ALT-PG2 was accompanied by an increase in the phosphorylated levels of AMP-activated protein kinase (AMPK), while phosphorylated extracellular-signal-regulated kinase 1/2 (ERK1/2) was reduced. Consistent with the key role of these kinases on endoplasmic reticulum (ER) stress, ALT-PG2 attenuated the levels of ER stress and inflammatory markers. Overall, the findings of this study indicate that targeting sEH with degraders is a promising pharmacological strategy to promote AMPK activation and to reduce ER stress and inflammation.

Keywords

sEH; PROTAC; AMPK; ER stress; hepatocyte

1. Introduction

Proteolysis-targeting chimeras (PROTACs) molecules have changed the landscape for drug discovery and design (1). PROTACs are bifunctional molecules consisting of a ligand targeting a protein of interest, a ligand recruiting an E3 ligase, and a connecting linker (1). Compared to classical inhibitors, PROTACs not only inhibit their targets, but also induce their degradation through the ubiquitin-proteasome system. This offers several advantages over merely inhibiting proteins, including the use of lower doses (2), and additional layer of selectivity (3), cumulative efficacy (4), and the potential to degrade undruggable targets and domains (5).

Soluble epoxide hydrolase (sEH) is a bifunctional enzyme with C-terminal hydrolase and N-terminal phosphatase activities (6). This enzyme is highly expressed in the liver (6), a vital organ with important metabolic, secretory and excretory functions. sEH hydrolase activity converts epoxyeicosatrienoic acids (EETs) and other epoxy fatty acids (EpFAs) to their corresponding diols. The products of hydrolysis of the EETs and other EpFAs are dihydroxyeicosatrienoic acids. These diols are much less bioactive than their parents epoxides. As a result, compounds that inhibit sEH significantly increase levels of EETs and other EpFAs, which are opposing counterparts to the largely pro-inflammatory prostanoids and leukotrienes, providing therapeutic efficacy for the treatment of neurodegenerative diseases, inflammation, chronic pain, cardiovascular disease, pulmonary diseases, and diabetes (7–9). Many of these chronic diseases are also the result of persistent endoplasmic reticulum (ER) stress due to its potential to elicit aberrant inflammatory signaling and facilitate cell death (10, 11). Thus, targeting ER stress has emerged as a therapeutic strategy for many disorders. ER stress develops in part because of the accumulation of misfolded and unfolded proteins in the ER lumen. This disrupts the homeostasis of this organelle and activates the unfolded protein response (UPR), intended to restore the ER's folding capacity, and mitigate stress (12). However, if ER homeostasis cannot be restored, inflammation and cell death are induced. Therefore, although the UPR forms part of an acute mechanism to re-establish the cellular homeostasis, when sustained chronically activated this response contributes to disease. The UPR involves the activation of three transmembrane proteins: inositol-requiring enzyme 1 (IRE-1), activating transcription factor 6 (ATF6), and protein kinase R (PKR)-like ER kinase (PERK). The latter phosphorylates the eukaryotic initiation

factor (eIF2 α) and attenuates protein translation, thereby reducing the number of new proteins entering the ER lumen. If UPR cannot restore ER homeostasis, apoptosis is induced by the PERK-eIF2 α pathway and the subsequent increase in ATF4 activity, which upregulates the expression of C/EBP homologous protein (CHOP). Moreover, the three branches of the UPR intersect with a variety of inflammatory and stress signaling systems, including the nuclear factor- κ B (NF- κ B) pathway (12) or the signal transducer and activator of transcription 3 (STAT3) pathway (13), thereby stimulating inflammation.

Since the liver has a large requirement for protein synthesis and folding, hepatocytes are enriched in ER and, thus, are more susceptible to ER perturbation and ER stress (14). Excessive ER stress contributes to the development of insulin resistance and type 2 diabetes mellitus (12) and activation of adenosine monophosphate-activated protein kinase (AMPK) has been reported to protect against insulin resistance by reducing ER stress (15, 16). In addition, the presence of an inhibitory crosstalk between AMPK and extracellular-signal-regulated kinase 1/2 (ERK1/2) contributes to the development of ER stress, since inhibition of ERK1/2 was found to improve AMPK pathway and to reverse ER stress-induced insulin resistance (15, 16).

In this work, we describe that the sEH-targeting PROTAC ALT-PG2 degrades this protein at low nanomolar concentration in the human hepatoma-derived Huh-7 cell line and in primary mouse hepatocytes. The degradation of the sEH protein in these cells was accompanied by AMPK activation, while phosphorylated ERK1/2 was reduced. Moreover, these changes resulted in a basal reduction of both ER stress and inflammatory markers, whereas an increase was observed in the levels of proteins involved in the insulin signaling pathway. Likewise, ALT-PG2 prevented the increase in ER stress induced by thapsigargin, an ER stressor which induces ER stress by inhibiting SERCA (sarco/endoplasmic reticulum Ca²⁺ ATPase) and, consequently, blocking the calcium entry into the ER lumen. Finally, two intraperitoneal administrations of ALT-PG2 for one single day resulted in rapid and robust degradation of sEH in the liver of mice, as well as the activation of AMPK and the reduction of the phosphorylated levels of ERK1/2. Overall, these findings indicate that targeting sEH with PROTACs leads to the degradation of this protein *in vitro* and *in vivo*, which in turn results in the activation of AMPK and the reduction of ER stress and inflammatory markers.

2. Materials and methods

2.1. General

Commercially available reagents and solvents were used without further purification unless stated otherwise. 400 MHz ¹H and 100.6 MHz ¹³C NMR spectra were recorded on a Bruker 400 Avance III spectrometers. The chemical shifts are reported in ppm (δ scale) relative to internal tetramethylsilane, and coupling constants are reported in Hertz (Hz). High resolution mass spectrometry (HRMS) analyses were performed with an LC/MSD TOF Agilent Technologies spectrometer. HPLC / MS were determined with a HPLC Agilent 1260 Infinity II LC/MSD coupled to a photodiode array and mass spectrometer. Samples (5 μ L, 0.5 mg/mL) in a 1:1 mixture of water with 0.05% formic acid (A) and acetonitrile with 0.05% formic acid (B) were injected using an Agilent Poroshell 120 EC-C18 (2.7 μ m, 50 mm \times 4.6 mm) column at 40 $^{\circ}$ C. The mobile phase was a mixture of A and B, with a flow

0.6 mL/min, using the following gradients: from 95% A–5% B to 100% B in 3 min; 100% B for 3 min; from 100% B to 95% A–5% B in 1 min; and 95% A–5% B for 3 min. Purity is given as % of absorbance at 254 nm. All compounds that were subjected to pharmacological evaluation are >95% pure by HPLC.

2.2 Synthesis procedure for PROTAC molecules

Synthesis of ALT-PG2.—To a solution of *trans*-4-[4-(3-trifluoromethoxyphenyl)-1-ureido)cyclohexyloxy]benzoic acid (*t*-TUCB) (26 mg, 0.055 mmol) in dimethylformamide (DMF) (0.5 mL) was added the recruiter molecule (thalidomide-PEG3-NH₂·HCl, 25 mg, 0.046 mmol), and the solution was stirred at room temperature. *N,N*-diisopropylethylamine (DIPEA) (24 μl, 0.138 mmol) was added dropwise, and the mixture was stirred for 5 min at room temperature. Hexafluorophosphate azabenzotriazole tetramethyl uronium (HATU) (35 mg, 0.092 mmol) was added, and the mixture was stirred at room temperature overnight. Water was added, and the mixture was extracted with ethyl acetate (3×). The combined organic phases were washed with NaHCO₃ (twice), dried over anhydrous Na₂SO₄, filtered, and evaporated under reduced pressure to give a crude. Column chromatography [SiO₂, 100% dichloromethane (DCM) to 90% DCM / 10% methanol mixtures] yielded ALT-PG2 (23 mg, 54% yield) as a white solid.

¹H-RMN (400 MHz, DMSO-*d*₆) δ: 1.32 – 1.40 (cs, 2H), 1.44 – 1.53 (cs, 2H), 1.91 – 1.95 (cs, 2H), 2.00 – 2.06 (cs, 3H), 2.51 – 2.50 (cs, 2H), 2.89 (ddd, *J* = 17.6, *J*' = 13.9, *J*'' = 5.5 Hz, 1H), 3.30 (s, 2H), 3.38 (q, *J* = 6.0 Hz, 2H), 3.44 (t, *J* = 5.6 Hz, 2H), 3.48–3.50 (cs, 12 H), 4.42 (m, 1H), 4.78 (s, 2H), 5.11 (dd, *J* = 13.2 Hz, *J*' = 3.6 Hz, 1H), 6.18 (d, *J* = 7.4 Hz, 1H), 6.99 (d, *J* = 8.8 Hz, 2H), 7.21 (d, *J* = 8.4 Hz, 2H), 7.39 (d, *J* = 8.4 Hz, 1H), 7.45–7.50 (cs, 3H), 7.77–7.82 (cs, 3H), 8.00 (t, *J* = 5.6 Hz, 1H), 8.32 (t, *J* = 5.6 Hz, 1H), 8.5 (s, 1H), 11.11 (brs, 1H).

¹³C-RMN (100.6 MHz, DMSO-*d*₆) δ: 22.0, 29.7, 30.0, 30.9, 38.4, 47.2, 48.8, 67.5, 68.8, 69.0, 69.6, 69.7, 74.1, 114.8, 116.0, 116.8, 118.5, 120.3, 121.6, 126.4, 129.0, 133.0, 136.9, 139.8, 141.9, 154.4, 155.0, 159.7, 165.4, 165.7, 166.7, 166.9, 169.9, 172.8.

HRMS-ESI- *m/z* [M-]⁻ calcd for [C₄₄H₄₈F₃N₆O₁₃]⁻: 925.3237, found: 925.3225.

Synthesis of ALT-PG3.—To a solution of *t*-TUCB (22 mg, 0.051 mmol) in DMF (0.5 ml) was added the recruiter molecule (thalidomide-PEG4-NH₂·HCl, 25 mg, 0.043 mmol), and the solution was stirred at room temperature. DIPEA (23 μl, 0.129 mmol) was added dropwise, and the mixture was stirred for 5 min at room temperature. HATU (33 mg, 0.086 mmol) was added, and the mixture was stirred at room temperature overnight. Water was added, and the mixture was extracted with ethyl acetate (3×). The combined organic phases were washed with NaHCO₃ (twice), dried over anhydrous Na₂SO₄, filtered, and evaporated under reduced pressure to give a crude. Column chromatography (SiO₂, 100% DCM to 90% DCM / 10% methanol mixtures) yielded ALT-PG3 (15 mg, 36% yield) as a white solid which spectroscopic data matched the described in the literature (17).

2.3. *In vitro* determination of the inhibitory activities toward human and mouse sEH

The *in vitro* inhibitory activity toward human and mouse sEH was determined as previously described (18).

2.4. Animal treatment

Male C57BL/6 mice (10–12 weeks old) were purchased from Envigo (Barcelona, Spain). After an acclimation period of 10 days, mice were randomly distributed into two experimental groups (n = 5 each). One of the groups received one i.p. injection of vehicle (0.9 % NaCl containing 5 % Kolliphor HS15 (42966, Sigma-Aldrich, St. Louis, MO, USA)) and the other ALT-PG2 (30 mg/kg, i.p., twice a day for 1 day) dissolved in the vehicle. Mice were sacrificed, and liver samples were frozen in liquid nitrogen and then stored at –80°C.

Animal experimentation complied with the Guide for the Care and Use of Laboratory Animals published by the US National Institutes of Health (8th edition: National Academies Press; 2011). All procedures were approved by the Bioethics Committee of the University of Barcelona, as stated in Law 5/21 July 1995 passed by the Generalitat de Catalunya. The animals were treated humanely, and all efforts were made to minimize both animal numbers and suffering.

2.5. Cell culture

Human Huh-7 hepatoma cells (kindly donated by Dr. Mayka Sanchez from the Josep Carreras Leukemia Research Institute, Barcelona) were cultured in DMEM supplemented with 10% fetal bovine serum and 1% penicillin-streptomycin, at 37°C under 5% CO₂.

Primary mouse hepatocytes were isolated from non-fasting male C57BL/6 mice (10–12 weeks old) by perfusion with collagenase as described elsewhere (19). Compounds ALT-PG2 and ALT-PG3 were dissolved in DMSO.

Huh-7 and mouse primary hepatocytes were exposed to ALT-PG2 for 48 h and co-incubated with vehicle (DMSO) or the ER stressor thapsigargin (1 μM) for the last 24 h.

2.6. Immunoblotting

Isolation of total protein extracts was performed as described elsewhere (20). Immunoblotting was performed with antibodies against AMPKα (#2532, Cell Signaling Technology, Danvers, MA, USA), phosphorylated AMPK Thr¹⁷² (#2531, Cell Signaling Technology), β-Actin (A5441, Sigma), CHOP (GTX112827, Genetex, Irvine, CA, USA), eIF2α (#9722, Cell Signalling Technology), phosphorylated eIF2α Ser⁵¹ (#9721, Cell Signalling Technology); ERK1/2 (44/42 MAPK) (#9102, Cell Signaling Technology), phosphorylated ERK1/2 (44/42 MAPK) Thr²⁰²/Tyr²⁰⁴ (#9101, Cell Signalling Technology), IRβ (#3025, Cell Signaling Technology), IRS-1 (#2382, Cell Signaling Technology), NF-κB p65 (sc-109, Santa Cruz Biotechnology Inc., Dallas, TX, USA), phosphorylated NF-κB p65 Ser⁵³⁶ (#3036s, Cell Signalling Technology), PP2A (#2259, Cell Signaling Technology), p53 (2524T, Cell Signaling Technology), sEH (sc-25797, Santa Cruz Biotechnology Inc.), SOCS3 (sc-9023, Santa Cruz Biotechnology Inc.), STAT3 (sc-482X, Santa Cruz Biotechnology Inc.), phosphorylated STAT3 Tyr⁷⁰⁵ (#9131, Cell Signaling Technology),

TNF- α (AF410-NA, R&D Systems, Minneapolis, MN, USA), TRB3 (sc-365842, Santa Cruz Biotechnology Inc.), vinculin (sc-25336, Santa Cruz Biotechnology Inc.), VLDLR (AF2258, R&D Systems). Signal acquisition was performed using the Amersham Imager 680 apparatus and quantification of the immunoblot signal was performed with the Bio-Rad Image Lab software. The results for protein quantification were normalized to the levels of a control protein to avoid unwanted sources of variation.

2.7. Statistical analysis

Results are expressed as the mean \pm SEM. Significant differences were assessed by either Student's t-test or one-way ANOVA, according to the number of groups compared, using the GraphPad Prism program (version 9.0.2) (GraphPad Software Inc., San Diego, CA, USA). When significant variations were found by ANOVA, Tukey's post-hoc test for multiple comparisons was performed only if F achieved a p value < 0.05 . Differences were considered significant at p < 0.05 .

3. Results

3.1. Synthesis and characterization of the sEH PROTAC ALT-PG2

Two sEH PROTACs were evaluated, ALT-PG2 and ALT-PG3. These compounds consist of the sEH competitive inhibitor *t*-TUCB (21) (Table 1) as binder to the enzyme, while incorporating the thalidomide-based cereblon ligand (as E3 ligase ligand) and two different polyethylene glycol (PEG) linkers. The synthesis of the targeted PROTACs was carried out by a coupling reaction of *t*-TUCB (21) and either thalidomide-PEG3-NH₂ for ALT-PG2, or thalidomide-PEG4-NH₂ for ALT-PG3, in the presence of HATU and DIPEA in DMF (Table 1). First, we examined the inhibitory activity of these compounds against the human and murine enzymes. Consistent with previous studies (17), and despite the presence of the bulky recruiter linked to the *t*-TUCB unit, the two compounds showed activity in the low nanomolar or even subnanomolar ranges in both the human and murine enzymes (Table 1). As a control, we first examined the effects of different concentrations of the sEH inhibitor *t*-TUCB on the protein levels of sEH in the human hepatoma-derived Huh-7 cell line. As expected, exposure to this compound did not cause sEH degradation (Figure 1A). In contrast, ALT-PG2 caused a robust degradation of sEH protein levels at concentrations ranging from 1 nM to 1 μ M (Figure 1B). At 1 μ M concentration some U-shaped concentration-response curve or hook effect was observed, a known phenomenon in PROTACs (22). This effect was not observed with ALT-PG3, although it caused a weaker degradation of sEH. Thus, we selected the ALT-PG2 PROTAC at 10 nM for further studies. When we conducted a time-course study, we observed that significant sEH degradation occurred after only 1 h of treatment, but exposure for longer periods (8, 12, and 24 h) provided greater degradation (Figure 1D). To determine whether ALT-PG2-induced proteasome-mediated degradation, cells were treated with the proteasome inhibitor MG132 prior PROTAC application. Inhibition of proteasome with MG132 completely abrogated the ALT-PG2-mediated degradation of sEH (Figure 2A), indicating that this degradation depends on the ubiquitin-proteasome system. Moreover, addition of the cereblon ligand lenalidomide effectively rescued the degradation of sEH by ALT-PG2, confirming that it requires the binding of ALT-PG2 to the E3 ligase cereblon (Figure 2B). One of the potential

advantages of PROTACs over inhibitors is the potential development of cumulative efficacy after repeated administration when the target protein has a slow turnover. To assess the presence of this potential effect for ALT-PG2, repeated administrations were conducted in cells. Exposure to 2 concentrations for 24 h or 4 concentrations for 12 h of 10 nM ALT-PG2 yielded similar degradations of sEH than a single concentration treatment (Figure 2C), suggesting that ALT-PG2 does not develop cumulative efficacy following repeated administrations, at least during the periods assessed.

3.2. sEH degradation by ALT-PG2 activates AMPK and reduces the levels of ER stress markers in human Huh-7 hepatic cells

Previous studies have reported that the reduction in cardiac AMPK caused by a high-fat diet (HFD) is prevented in sEH knockout mice (23), that hepatocytes from sEH knockout mice show activation of AMPK (24), as well as that sEH inhibition significantly attenuates the HFD-induced renal injury, partially by activating AMPK (25). Since these findings suggested that both the absence of sEH or its inhibition resulted in AMPK activation, we next examined whether sEH degradation by ALT-PG2 activated AMPK in human Huh-7 hepatic cells. Moreover, given that AMPK activation mitigates ER stress (15, 16), we also examined if ALT-PG2 attenuated ER stress and inflammatory markers. As expected, exposure of Huh-7 cells to 10 nM ALT-PG2 for 16 h caused a rapid and robust degradation of sEH (Figure 3A). This was accompanied by AMPK activation (Figure 3B), and consistent with the reported inhibitory crosstalk between AMPK and ERK1/2, the phosphorylated levels of the latter kinase were reduced (Figure 3C). The fact that the sEH inhibitor *t*-TUCB increased the phosphorylated levels of AMPK (Figure 3D) suggests that AMPK activation caused by ALT-PG2 is mediated by the reduction of the hydrolase levels, while further studies are needed to evaluate whether the phosphatase activity of the enzyme contributes to AMPK activation. AMPK is known to inhibit the p53 negative regulator, murine double minute X (MDMX), resulting in increased p53 levels (26). Consistent with this, AMPK activation caused by ALT-PG2 was accompanied by an increase in p53 protein levels (Figure 3E) supporting that ALT-PG2 activates AMPK. Likewise, treatment with ALT-PG2 reduced the levels of ER stress marker phosphorylated eIF2 α (Figure 3F), while no changes were observed in the levels of inflammatory transcription factor NF- κ B or its phosphorylation status (Figure 3G). Despite this latter finding, the levels of phosphorylated STAT3, which is activated by ER stress (13) and is the primary downstream regulator of interleukin (IL)-6 signaling with a prominent role in regulating inflammation (27), were attenuated by ALT-PG2 (Figure 3H). Since activation of the STAT3 pathway has been reported to reduce insulin receptor substrate 1 (IRS1) protein levels in hepatocytes (28) and ER stress reduces the levels of insulin receptor β (IR β) (29), we examined the levels of these two proteins involved in the insulin signaling pathway. Remarkably, the protein levels of both IR β and IRS1 were upregulated by ALT-PG2 (Figure 3I). Collectively, these findings indicate that the degradation of sEH by ALT-PG2 activates AMPK, reduces ER stress and inflammatory markers and increases the levels of proteins involved in the insulin signaling pathway in hepatocytes.

3.3. sEH degradation by ALT-PG2 attenuates thapsigargin-induced ER stress in human Huh-7 hepatic cells

To confirm that ALT-PG2 ameliorates ER stress, we used the ER stressor thapsigargin. Exposure of Huh-7 cells to thapsigargin did not significantly increase sEH protein levels (Figure 4A). Moreover, ALT-PG2 treatment resulted in sEH degradation independently of the presence of thapsigargin. Interestingly, ALT-PG2 abolished the thapsigargin-mediated increase in the ER stress markers CHOP (Figure 4A), phosphorylated eIF2 α (Figure 4B), tribbles 3 (TRB3) and very low-density lipoprotein receptor (VLDLR) (Figure 4C). Consistent with these effects of ALT-PG2, this PROTAC prevented the increase in the levels of suppressor of cytokine signaling 3 (SOCS3) (Figure 4A), a STAT3-target gene, and of the inflammatory markers p65-NF- κ B and TNF- α (Figure 4C). These findings indicate that ALT-PG2 reduces the levels of ER stress and inflammatory markers in thapsigargin-stimulated cells. Since AMPK activation prevents ER stress (15, 16), we examined whether the increase in AMPK activity caused by ALT-PG2 was responsible for the reduction of ER stress by using the AMPK inhibitor compound C. Remarkably, the reduction in CHOP protein levels caused by ALT-PG2 in thapsigargin-stimulated cells was prevented when cells were co-incubated with compound C (Figure 4D). This finding suggests that the inhibition of ER stress provoked by ALT-PG2 is mediated by AMPK.

3.4. sEH degradation by ALT-PG2 activates AMPK and reduces the levels of ER stress markers in mouse primary hepatocytes

Since primary hepatocytes are the gold standard for physiologically relevant *in vitro* liver models as they retain *in vivo*-like functions and morphologies, we next evaluated the effects of the ALT-PG2 PROTAC in this model. Exposure of mouse primary hepatocytes to ALT-PG2 led to significant sEH degradation (Figure 5A), which was accompanied by an increase in phosphorylated AMPK (Figure 5B). Likewise, and in agreement with the activation of AMPK, phosphorylated ERK1/2 was reduced (Figure 5C). In addition, ALT-PG2 reduced basal CHOP protein levels (Figure 5E), as well as the levels of SOCS3, while the protein levels of IR β were increased (Figure 5E). Likewise, when mouse primary hepatocytes were stimulated with thapsigargin, co-incubation of the cells with ALT-PG2 attenuated the increase in CHOP caused by the ER stressor (Figure 5F). In agreement with the reduction in ER stress, ALT-PG2 also reduced the levels of the inflammatory marker TNF- α (Figure 5G).

3.5. ALT-PG2 leads to sEH degradation in the liver of mice

We conducted a first approach to evaluate the effect of ALT-PG2 on sEH degradation *in vivo*. Mice treated with ALT-PG2 (30 mg/kg, twice a day for 1 day) showed a significant degradation in hepatic sEH protein levels (Figure 6A). Consistent with previous studies *in vitro*, ALT-PG2 increased the phosphorylated levels of AMPK in the liver (Figure 6B). The activation of AMPK was confirmed by the reduction in phosphorylated ERK1/2 (Figure 6C) and SOCS3 (Figure 6D). Collectively, these findings suggest that the PROTAC ALT-PG2 causes a potent and rapid degradation of sEH *in vivo* after only 24 h that results in the activation of AMPK.

4. Discussion

In the present study we show that the ALT-PG2 PROTAC (based on the scaffold of the sEH inhibitor *t*-TUCB connected to thalidomide-like ligand as the recruiter of the E3 ligase cereblon and a PEG linker) degrades sEH in the human Huh-7 hepatic cell line, in mouse primary hepatocytes and in mouse liver. In addition, sEH degradation results in the activation of AMPK and the reduction of phosphorylated ERK1/2, which are important regulators of ER stress. In fact, ALT-PG2 reduces basal ER stress markers after stimulation with an ER stressor. Moreover, the inhibition of ER stress caused by ALT-PG2 seems to be mediated by the activation of AMPK. The effects of ALT-PG2 also contribute to attenuate inflammation and the increase in the levels of proteins involved in the insulin signaling pathway, suggesting that ALT-PG2 might be a potential treatment of insulin resistance and type 2 diabetes mellitus as well as metabolic diseases associated with these conditions. In our study we have also assessed another PROTAC, ALT-PG3, which yielded a slightly lower degradation of sEH than ALT-PG2. Indeed, ALT-PG3 has been previously evaluated in a recent study designed as compound **1a** (17). Interestingly, this study elegantly demonstrated that ALT-PG3 selectively targeted the degradation of cytosolic but not peroxisomal sEH. It is also reported that the lack of effect of ALT-PG3 on peroxisomal sEH explained the apparent lack of total degradation of sEH. Given the structural similarities between ALT-PG2 and ALT-PG3, it is likely that ALT-PG2 may also show selectivity against cytosolic sEH, thereby explaining the lack of total degradation of this protein. However, despite the structural similarities, some differences may exist between ALT-PG2 and ALT-PG3. In fact, according to this previous study, ALT-PG3-mediated sEH degradation was not rescued by the proteasome inhibitor MG132. However, they observed that the lysosomal pathway was involved in the ALT-PG3-mediated degradation of sEH (17). In contrast, we report that MG132 rescues completely the degradation of sEH caused by ALT-PG2, indicating that ALT-PG2-mediated sEH degradation involves the proteasome system. We do not know the reasons for these differences between ALT-PG2 and ALT-PG3, but the use of different cell lines (Huh-7 in our study vs. HepG2 and HEK293T) or concentrations (10 nM ALT-PG2 in our study vs. 250 nM ALT-PG3) might contribute, since, for instance, it is well-known in the field the influence of the cell line in the degradation patterns.

We also show that sEH degradation by ALT-PG2 activates AMPK *in vitro* and *in vivo*. In fact, previous studies have observed AMPK activation in the sEH knockout mice (23, 24) and following treatment with sEH inhibitors (25). Our findings confirm that sEH degradation by PROTAC is also a valid strategy to activate AMPK in hepatic cells. This has implications for the treatment of insulin resistance and type 2 diabetes mellitus, since the most prescribed drug for the treatment of type 2 diabetes mellitus, metformin, activates AMPK. Moreover, due to the presence of an inhibitory crosstalk between AMPK and ERK1/2, activation of AMPK by ALT-PG2 might be responsible for the reduction of ER stress, since it has been reported that inhibition of ERK1/2 reverses ER stress-induced insulin resistance (15, 16). Actually, our findings demonstrate that AMPK activation by ALT-PG2 is required for the inhibition of ER stress, since the AMPK inhibitor compound C abolished this effect. It is well-known that ER stress contributes to insulin resistance and type 2 diabetes by activating inflammatory pathways and by reducing the protein levels of

key proteins of the insulin-signaling pathway (12). In fact, our findings show that AMPK activation by ALT-PG2-mediated degradation of sEH results in a reduction of inflammatory markers. Since ER stress has been reported to reduce IR β levels (29), the reduction in ER stress caused by ALT-PG2 might be responsible for the increase in the levels of this receptor. Similarly, ALT-PG2 reduces the activation of STAT3 and the levels of its target gene SOCS3. Given that the STAT3-SOCS3 pathway reduces hepatic IRS1 levels (28), its attenuation by ALT-PG2 could be the underlying mechanism responsible for the increase in IR β levels. Moreover, because of AMPK activation following sEH degradation, p53 protein levels were also increased. This result is relevant since it has been reported that p53 modulates hepatic insulin sensitivity through NF- κ B and p38/ERK-mitogen activated protein kinase (MAPK) pathways (30).

As far as we know, this is the first study reporting the efficacy of a PROTAC to promote the degradation of sEH *in vivo*. Further studies are necessary to better characterize the effects of PROTACs targeting sEH, but this first approach provides some interesting data. Our findings confirm that targeting sEH degradation by using degraders leads to AMPK activation after an acute treatment. Likewise, the activation of AMPK by ALT-PG2 in the liver results in a reduction of phosphorylated ERK1/2 and SOCS3 levels, indicating that ALT-PG2 shows beneficial effects similar to those observed in Huh-7 cells and in primary hepatocytes. A previous study has reported that AMPK activation in the liver of sEH knockout mice was elicited by higher levels of the sEH substrate 12,13-epoxyoctadecenoic acid (24). Although we have not examined the levels of this substrate, it is likely that the level of degradation of sEH caused by ALT-PG2 might be sufficient to increase the levels of 12,13-epoxyoctadecenoic acid, eventually leading to the activation of AMPK.

Altogether, the findings of this study demonstrate that the ALT-PG2 PROTAC degrades sEH protein in human Huh-7 hepatic cells, mouse primary hepatocytes, and in the liver of mice. In these three models the degradation of sEH was accompanied by the activation of AMPK and the reduction of phosphorylated ERK1/2 as well as the reduction of ER stress and inflammatory markers. These findings indicate that targeting sEH with a PROTAC molecule is an effective strategy to activate AMPK and to prevent ER stress and inflammation in hepatic cells.

Acknowledgements

We would like to thank the Language Services of the University of Barcelona for revising the manuscript.

Funding

This study was partly supported by grants RTI2018-093999-B-100 and PID2021-122116OB-I00 (M.V.-C.), PID2020-118127RB-I00 (S.V.) and PID2021-122766OB-I00 (A.M.V.) funded by MCIN/AEI/10.13039/501100011033 and by “ERDF A way of making Europe”. CIBER de Diabetes y Enfermedades Metabólicas Asociadas (CIBERDEM) is a Carlos III Health Institute project. CERCA Programme/Generalitat de Catalunya. Partial support was provided by NIH – NIEHS (RIVER Award) R35 ES030443-01, NIH – NIEHS (Superfund Award) P42 ES004699 and NIH Counter Act Award U54 NS127758 (B.H.).

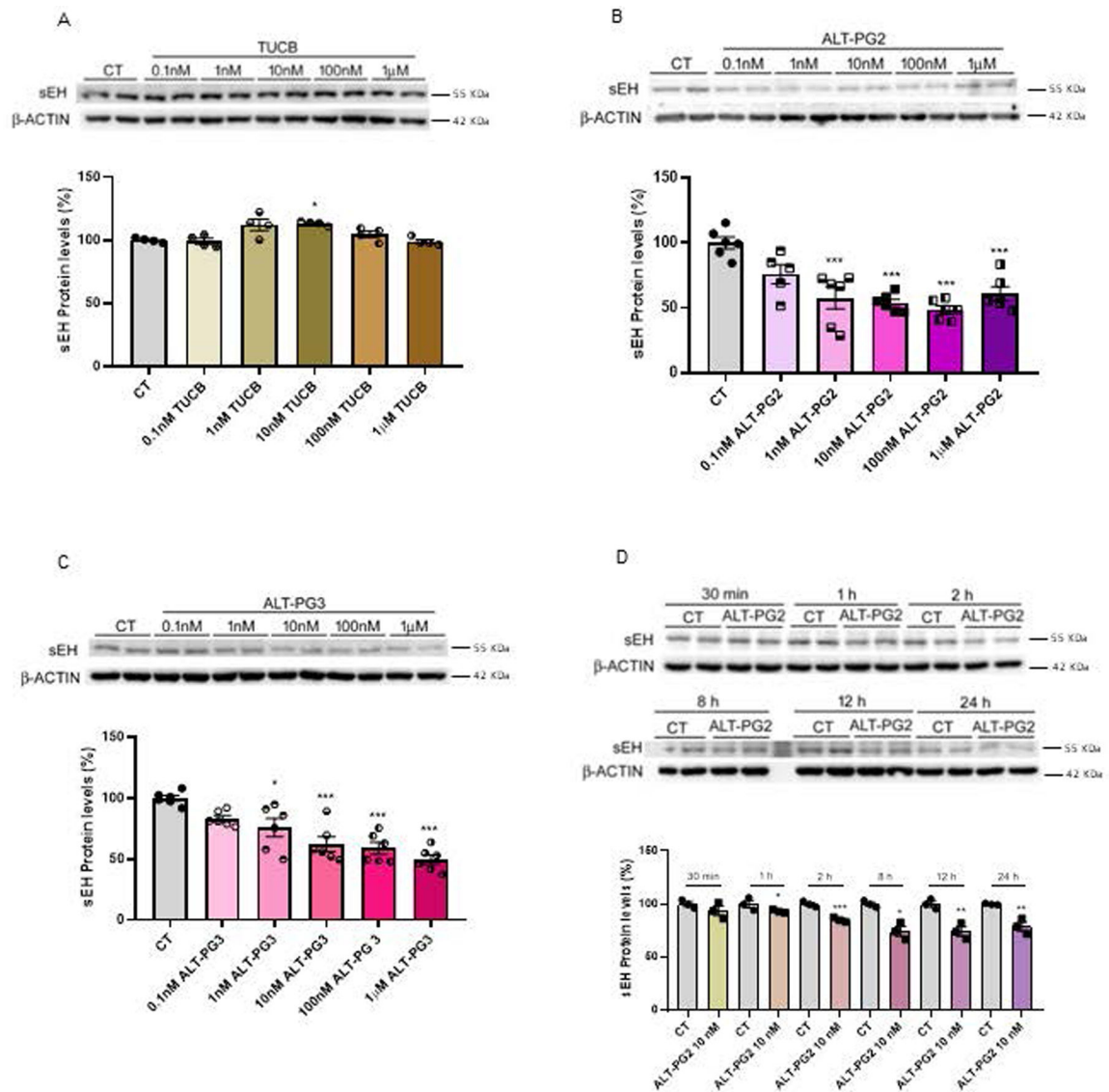
Data Availability

The study data are available on demand.

References

1. Bekes M, Langley DR, Crews CM. PROTAC targeted protein degraders: the past is prologue. *Nat Rev Drug Discov* 2022;21(3):181–200. [PubMed: 35042991]
2. Zou Y, Ma D, Wang Y. The PROTAC technology in drug development. *Cell Biochem Funct* 2019;37(1):21–30. [PubMed: 30604499]
3. Rana S, Bendjennat M, Kour S, King HM, Kizhake S, Zahid M, Natarajan A. Selective degradation of CDK6 by a palbociclib based PROTAC. *Bioorg Med Chem Lett* 2019;29(11):1375–1379. [PubMed: 30935795]
4. Mares A, Miah AH, Smith IED, Rackham M, Thawani AR, Cryan J, Haile PA, Votta BJ, Beal AM, Capriotti C, Reilly MA, Fisher DT, Zinn N, Bantscheff M, MacDonald TT, Vossenkamper A, Dace P, Churcher I, Benowitz AB, Watt G, Denyer J, Scott-Stevens P, Harling JD. Extended pharmacodynamic responses observed upon PROTAC-mediated degradation of RIPK2. *Commun Biol* 2020;3(1):140. [PubMed: 32198438]
5. Kargbo RB. PROTAC-Mediated Degradation of KRAS Protein for Anticancer Therapeutics. *ACS Med Chem Lett* 2020;11(1):5–6. [PubMed: 31938454]
6. Newman JW, Morisseau C, Harris TR, Hammock BD. The soluble epoxide hydrolase encoded by EPXH2 is a bifunctional enzyme with novel lipid phosphate phosphatase activity. *Proc Natl Acad Sci U S A* 2003;100(4):1558–1563. [PubMed: 12574510]
7. van Bussel FCG, Backes WH, Hofman PAM, van Oostenbrugge RJ, van Boxtel MPJ, Verhey FRJ, Steinbusch HWM, Schram MT, Stehouwer CDA, Wildberger JE, Jansen JFA. Cerebral Pathology and Cognition in Diabetes: The Merits of Multiparametric Neuroimaging. *Front Neurosci* 2017;11:188. [PubMed: 28424581]
8. Wagner KM, McReynolds CB, Schmidt WK, Hammock BD. Soluble epoxide hydrolase as a therapeutic target for pain, inflammatory and neurodegenerative diseases. *Pharmacol Ther* 2017;180:62–76. [PubMed: 28642117]
9. Kodani SD, Hammock BD. The 2014 Bernard B. Brodie award lecture-epoxide hydrolases: drug metabolism to therapeutics for chronic pain. *Drug Metab Dispos* 2015;43(5):788–802. [PubMed: 25762541]
10. Chadwick SR, Lajoie P. Endoplasmic Reticulum Stress Coping Mechanisms and Lifespan Regulation in Health and Diseases. *Front Cell Dev Biol* 2019;7:84. [PubMed: 31231647]
11. Bettaieb A, Nagata N, AbouBechara D, Chahed S, Morisseau C, Hammock BD, Haj FG. Soluble epoxide hydrolase deficiency or inhibition attenuates diet-induced endoplasmic reticulum stress in liver and adipose tissue. *J Biol Chem* 2013;288(20):14189–14199. [PubMed: 23576437]
12. Salvado L, Palomer X, Barroso E, Vazquez-Carrera M. Targeting endoplasmic reticulum stress in insulin resistance. *Trends Endocrinol Metab* 2015;26(8):438–448. [PubMed: 26078196]
13. Meares GP, Liu Y, Rajbhandari R, Qin H, Nozell SE, Mobley JA, Corbett JA, Benveniste EN. PERK-dependent activation of JAK1 and STAT3 contributes to endoplasmic reticulum stress-induced inflammation. *Mol Cell Biol* 2014;34(20):3911–3925. [PubMed: 25113558]
14. Liu X, Green RM. Endoplasmic reticulum stress and liver diseases. *Liver Res* 2019;3(1):55–64. [PubMed: 32670671]
15. Hwang SL, Jeong YT, Li X, Kim YD, Lu Y, Chang YC, Lee IK, Chang HW. Inhibitory cross-talk between the AMPK and ERK pathways mediates endoplasmic reticulum stress-induced insulin resistance in skeletal muscle. *Br J Pharmacol* 2013;169(1):69–81. [PubMed: 23373714]
16. Salvado L, Barroso E, Gomez-Foix AM, Palomer X, Michalik L, Wahli W, Vazquez-Carrera M. PPARbeta/delta prevents endoplasmic reticulum stress-associated inflammation and insulin resistance in skeletal muscle cells through an AMPK-dependent mechanism. *Diabetologia* 2014;57(10):2126–2135. [PubMed: 25063273]
17. Wang Y, Morisseau C, Takamura A, Wan D, Li D, Sidoli S, Yang J, Wolan DW, Hammock BD, Kitamura S. PROTAC-Mediated Selective Degradation of Cytosolic Soluble Epoxide Hydrolase Enhances ER Stress Reduction. *ACS Chem Biol* 2023;18(4):884–896. [PubMed: 36947831]
18. Jones PD, Wolf NM, Morisseau C, Whetstone P, Hock B, Hammock BD. Fluorescent substrates for soluble epoxide hydrolase and application to inhibition studies. *Anal Biochem* 2005;343(1):66–75. [PubMed: 15963942]

19. Benveniste R, Danoff TM, Ilekis J, Craig HR. Epidermal growth factor receptor numbers in male and female mouse primary hepatocyte cultures. *Cell Biochem Funct* 1988;6(4):231–235. [PubMed: 3191582]
20. Aguilar-Recarte D, Barroso E, Zhang M, Rada P, Pizarro-Delgado J, Pena L, Palomer X, Valverde AM, Wahli W, Vazquez-Carrera M. A positive feedback loop between AMPK and GDF15 promotes metformin antidiabetic effects. *Pharmacol Res* 2022;187:106578. [PubMed: 36435271]
21. Hwang SH, Tsai HJ, Liu JY, Morisseau C, Hammock BD. Orally bioavailable potent soluble epoxide hydrolase inhibitors. *J Med Chem* 2007;50(16):3825–3840. [PubMed: 17616115]
22. Pettersson M, Crews CM. PROteolysis TArgeting Chimeras (PROTACs) - Past, present and future. *Drug Discov Today Technol* 2019;31:15–27. [PubMed: 31200855]
23. Wang L, Zhao D, Tang L, Li H, Liu Z, Gao J, Edin ML, Zhang H, Zhang K, Chen J, Zhu X, Wang D, Zeldin DC, Hammock BD, Wang J, Huang H. Soluble epoxide hydrolase deficiency attenuates lipotoxic cardiomyopathy via upregulation of AMPK-mTORC mediated autophagy. *J Mol Cell Cardiol* 2021;154:80–91. [PubMed: 33378686]
24. Mangels N, Awwad K, Wettenmann A, Dos Santos LR, Fromel T, Fleming I. The soluble epoxide hydrolase determines cholesterol homeostasis by regulating AMPK and SREBP activity. *Prostaglandins Other Lipid Mediat* 2016;125:30–39. [PubMed: 27179554]
25. Luo Y, Wu MY, Deng BQ, Huang J, Hwang SH, Li MY, Zhou CY, Zhang QY, Yu HB, Zhao DK, Zhang G, Qin L, Peng A, Hammock BD, Liu JY. Inhibition of soluble epoxide hydrolase attenuates a high-fat diet-mediated renal injury by activating PAX2 and AMPK. *Proc Natl Acad Sci U S A* 2019;116(11):5154–5159. [PubMed: 30804206]
26. Aguilar-Recarte D, Barroso E, Guma A, Pizarro-Delgado J, Pena L, Ruat M, Palomer X, Wahli W, Vazquez-Carrera M. GDF15 mediates the metabolic effects of PPARbeta/delta by activating AMPK. *Cell Rep* 2021;36(6):109501. [PubMed: 34380027]
27. Matsuda T The Physiological and Pathophysiological Role of IL-6/STAT3-Mediated Signal Transduction and STAT3 Binding Partners in Therapeutic Applications. *Biol Pharm Bull* 2023;46(3):364–378. [PubMed: 36858565]
28. Serrano-Marco L, Barroso E, El Kochairi I, Palomer X, Michalik L, Wahli W, Vazquez-Carrera M. The peroxisome proliferator-activated receptor (PPAR) beta/delta agonist GW501516 inhibits IL-6-induced signal transducer and activator of transcription 3 (STAT3) activation and insulin resistance in human liver cells. *Diabetologia* 2012;55(3):743–751. [PubMed: 22179221]
29. Zhou L, Zhang J, Fang Q, Liu M, Liu X, Jia W, Dong LQ, Liu F. Autophagy-mediated insulin receptor down-regulation contributes to endoplasmic reticulum stress-induced insulin resistance. *Mol Pharmacol* 2009;76(3):596–603. [PubMed: 19541767]
30. Geng S, Zhu W, Wang S, Xie C, Li X, Wu J, Li Y, Chen Y, Wang X, Meng Y, Zhang Q, Chen J, Zhong C. P53 modulates hepatic insulin sensitivity through NF-kappaB and p38/ERK MAPK pathways. *Biochem Biophys Res Commun* 2018;495(3):2139–2144. [PubMed: 29258820]

**Figure 1.**

ALT-PG2 PROTAC degrades sEH in Huh-7 hepatic cells.

(A) Immunoblot analysis of sEH in Huh-7 hepatic cells exposed to different concentrations of *l*-TUCB for 24 h. Immunoblot analysis of sEH in Huh-7 hepatic cells exposed to different concentrations of (B) ALT-PG2 or (C) ALT-PG3 for 24 h. (D) Time-course of the effects of 10 nM ALT-PG2 on sEH protein levels. Data are presented as the mean \pm SEM. one-way ANOVA with Tukey's post hoc test. * $p < 0.05$, ** $p < 0.01$ and *** $p < 0.001$ vs. control (CT).

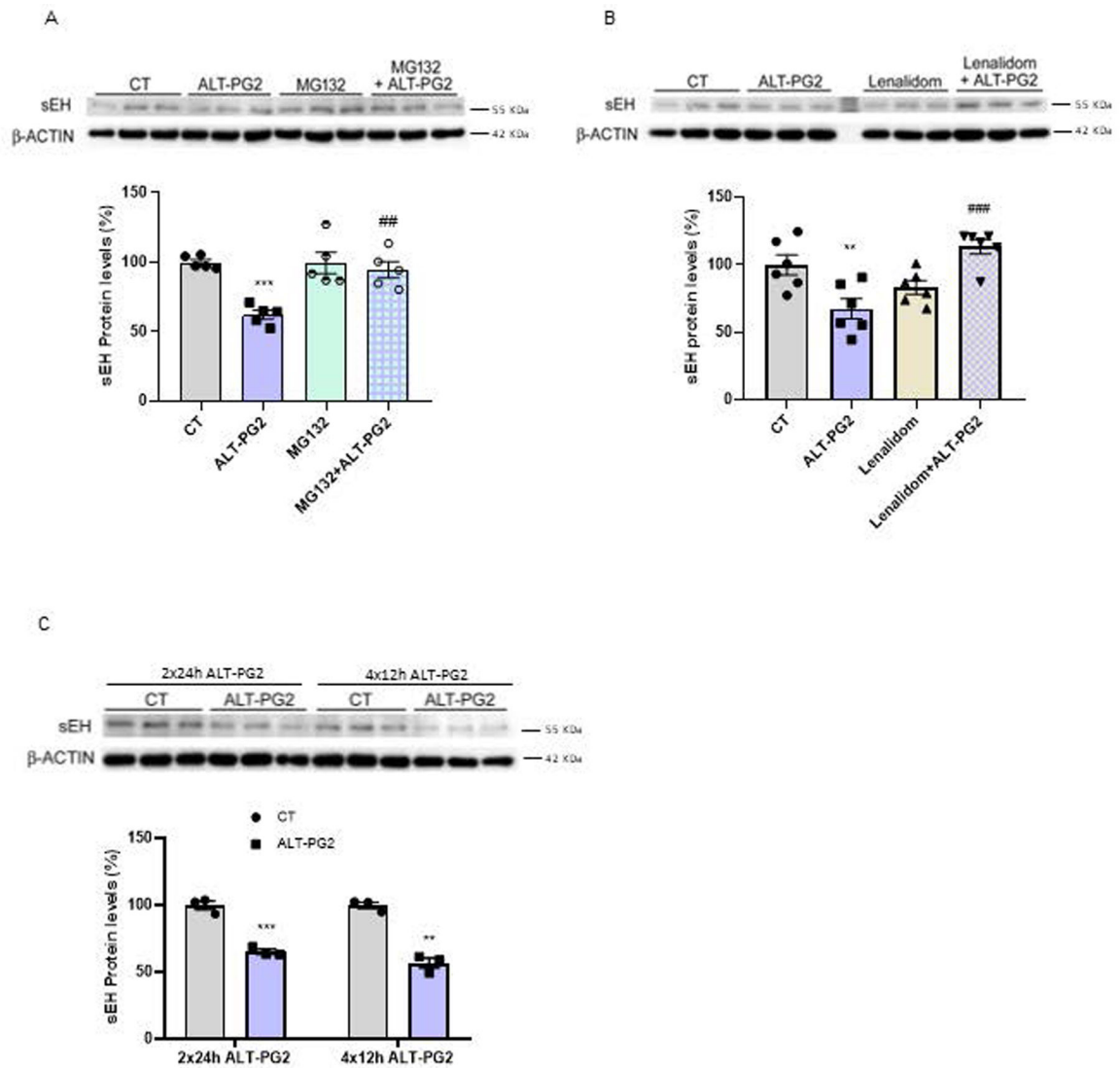


Figure 2.

ALT-PG2 degrades sEH via the ubiquitin–proteasome system in Huh-7 hepatic cells.

(A) Immunoblot analysis of sEH in Huh-7 hepatic cells exposed to 10 nM ALT-PG2 for 24 h in the presence or in the absence of 10 μ M of the proteasome inhibitor MG132 (added 3 h prior ALT-PG2). (B) Immunoblot analysis of sEH in Huh-7 hepatic cells exposed to 10 nM ALT-PG2 for 24 h in the presence or in the absence of 100 μ M of the cereblon ligand lenalidomide (added 3 h prior ALT-PG2). (C) sEH protein levels in Huh-7 hepatic cells exposed to the addition of 2 concentrations of ALT-PG2, each one every 24 h, and 4 concentrations of ATL-PG2, each one every 12 h. Data are presented as the mean \pm SEM. Significant differences were established by Student's-t test or one-way ANOVA with Tukey's post hoc test. * $p < 0.05$, ** $p < 0.01$ and *** $p < 0.001$ vs. CT. # $p < 0.05$, and ### $p < 0.01$ vs. ALT-PG2.

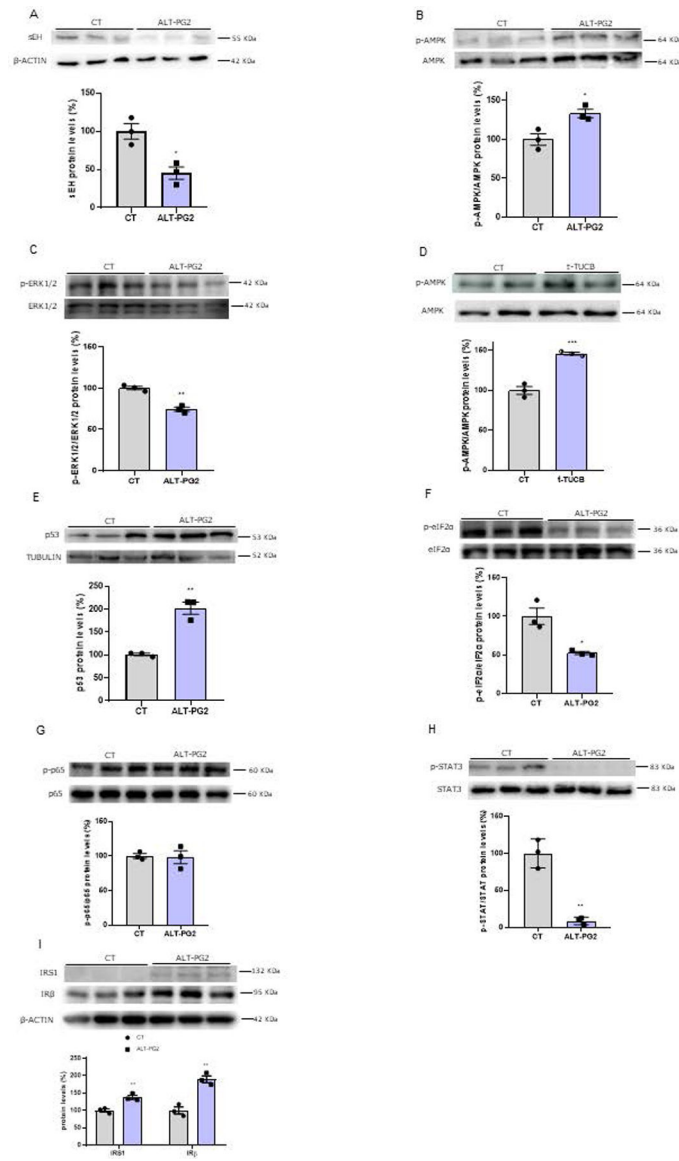


Figure 3.

sEH degradation by ALT-PG2 activates AMPK and reduces basal levels of ER stress markers in Huh-7 hepatic cells.

Immunoblot analysis of (A) sEH in Huh-7 hepatic cells exposed to 10 nM ALT-PG2 for 16 h. (B) Total and phosphorylated AMPK and (C) total and phosphorylated ERK1/2 in Huh-7 hepatic cells exposed to 10 nM ALT-PG2 for 48 h. (D) Immunoblot analysis of total and phosphorylated AMPK in Huh-7 hepatic cells exposed to 1 μ M *ε*-TUCB for 4 h. Immunoblot analysis of (E) p53, (F) total and phosphorylated eIF2 α , (G) total and phosphorylated levels of the p65 subunit of NF- κ B, (H) total and phosphorylated (Tyr⁷⁰⁵) levels of STAT3 and (I) IR β and IRS1 in Huh-7 hepatic cells exposed to 10 nM ALT-PG2 for 16 h. Significant differences were established by Student's-t test. *p < 0.05, **p < 0.01 and ***p < 0.001 vs. CT.

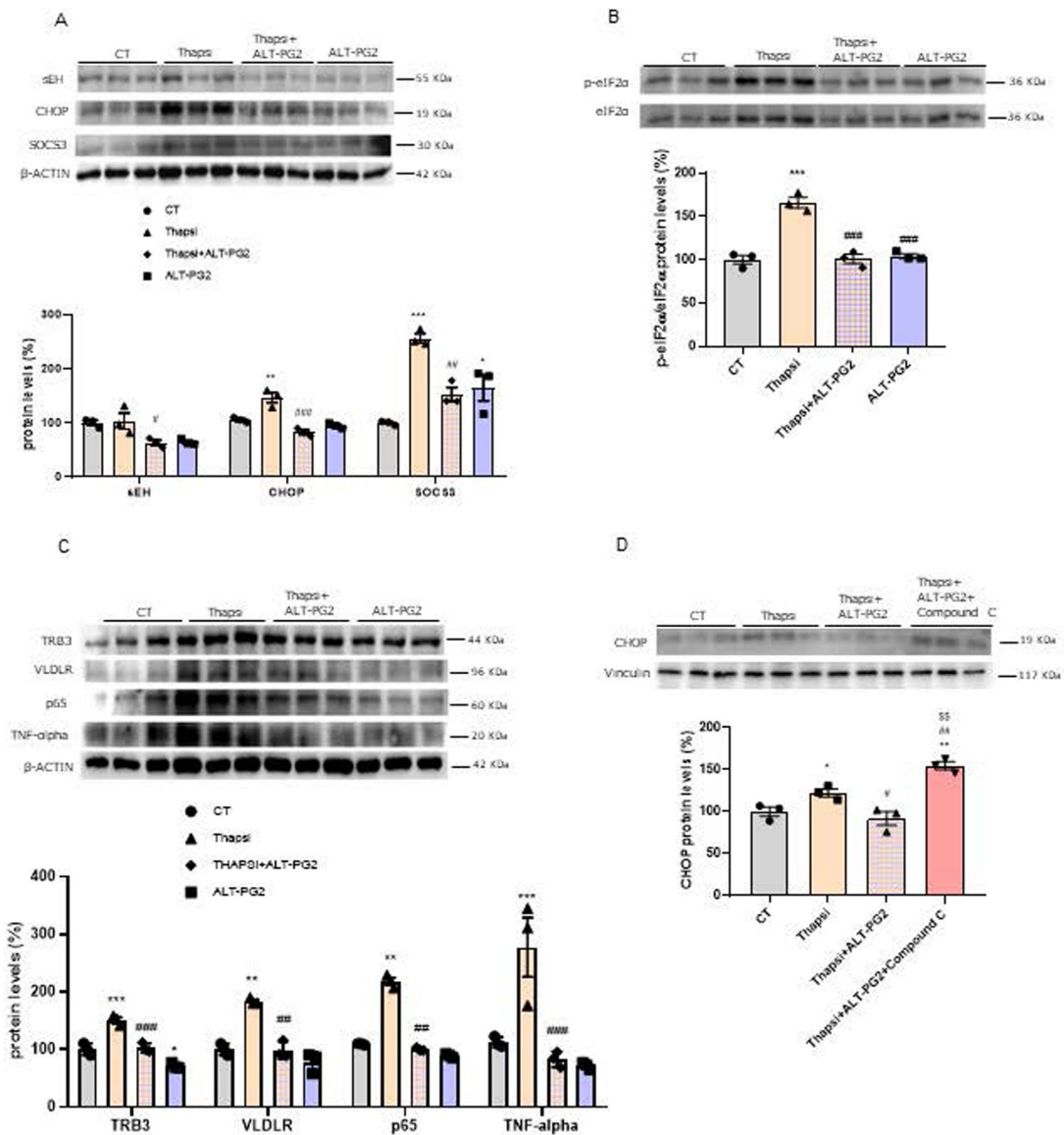


Figure 4. sEH degradation by ALT-PG2 attenuates thapsigargin-induced ER stress in Huh-7 hepatic cells.

Immunoblot analysis of (A) sEH, CHOP, SOCS3 and (B) total and phosphorylated eIF2α in Huh-7 hepatic cells exposed to 10 nM ALT-PG2 for 48 h co-incubated with vehicle or the ER stressor thapsigargin (1 μM) for the last 24 h. (C) TRB3, VLDLR, p65 and TNF-α in Huh-7 hepatic cells exposed to 10 nM ALT-PG2 for 48 h co-incubated with vehicle or the ER stressor thapsigargin (1 μM) for the last 24 h. (D) Immunoblot analysis of CHOP in Huh-7 hepatic cells exposed to 10 nM ALT-PG2 for 48 h co-incubated with vehicle or the ER stressor thapsigargin (1 μM) for the last 24 h with or without the AMPK inhibitor compound C (15 μM). Data are presented as the mean ± SEM. Significant differences were established by one-way ANOVA with Tukey’s post hoc test. *p < 0.05, **p < 0.01 and ***p < 0.001.

< 0.001 vs. CT. #p < 0.05, ##p < 0.01 and ###p < 0.001 vs. thapsigargin. \$\$p < 0.01 vs. Thapsi+ALT-PG2.

Author Manuscript

Author Manuscript

Author Manuscript

Author Manuscript

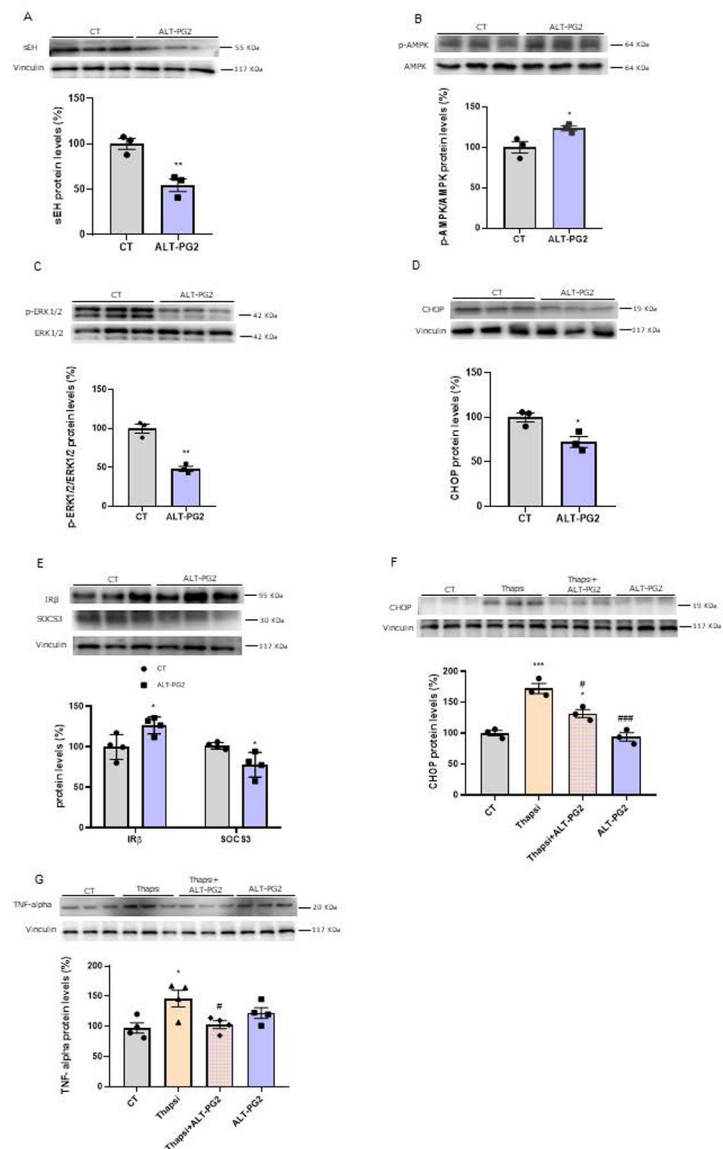


Figure 5.

sEH degradation by ALT-PG2 attenuates ER stress in mouse primary hepatocytes. Immunoblot analysis of (A) sEH, (B) total and phosphorylated AMPK, (C) total and phosphorylated ERK1/2, (D) CHOP, (E) IR β and SOCS3 in mouse primary hepatocytes exposed to 10 nM ALT-PG2 for 48 h. Immunoblot analysis of (F) CHOP and (G) TNF- α in mouse primary hepatocytes exposed to 10 nM ALT-PG2 for 48 h co-incubated with vehicle or the ER stressor thapsigargin (1 μ M) for the last 24 h. Data are presented as the mean \pm SEM. Significant differences were established by Student's-t test or one-way ANOVA with Tukey's post hoc test. * $p < 0.05$, ** $p < 0.01$ and *** $p < 0.001$ vs. CT. # $p < 0.05$ and ### $p < 0.001$ vs. thapsigargin.

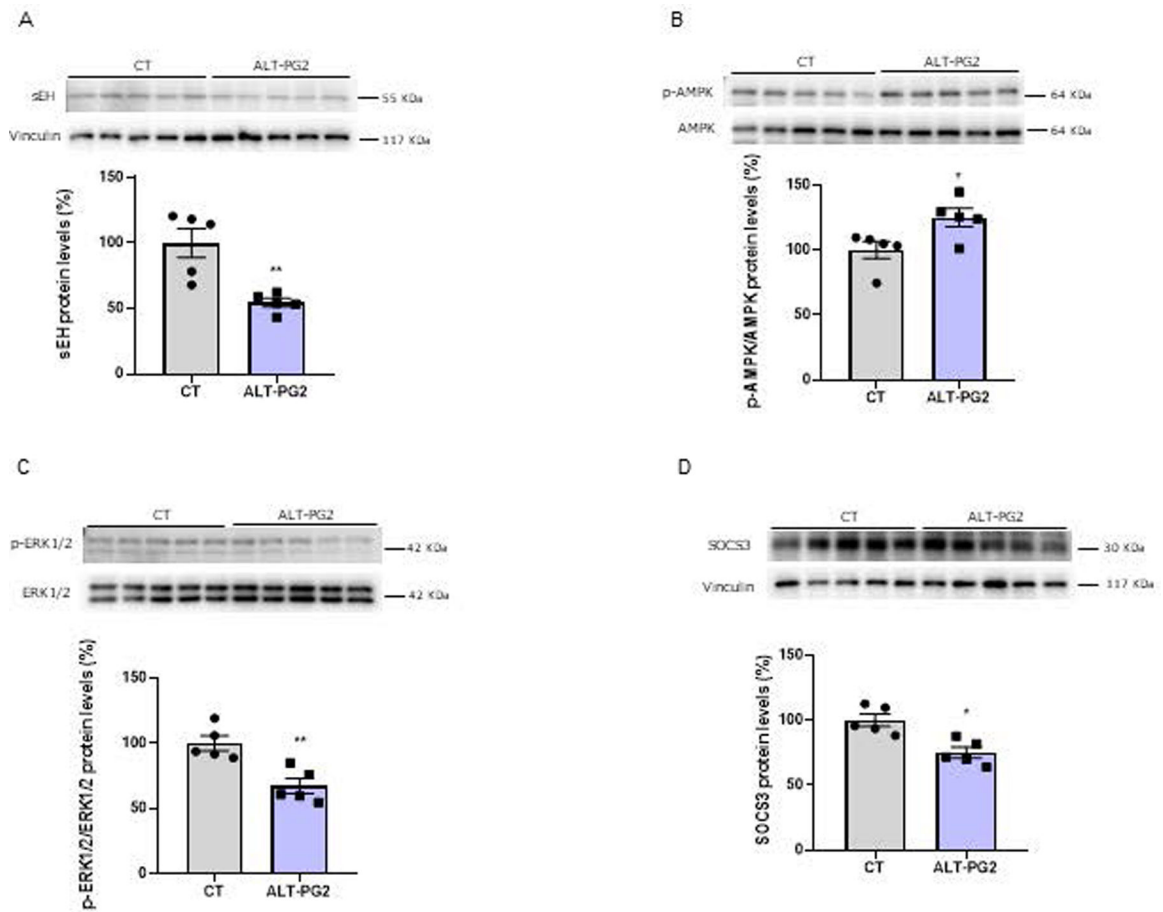
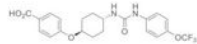
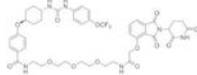
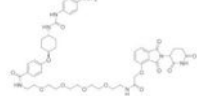


Figure 6.

ALT-PG2 degrades sEH *in vivo*.

Immunoblot analysis of (A) sEH, (B) total and phosphorylated AMPK, (C) total and phosphorylated ERK1/2, (D) SOCS3 in the liver of mice treated with vehicle or ALT-PG2 (30 mg/kg, i.p., twice a day for 1 day). Significant differences were established by Student's-t test. * $p < 0.05$ and ** $p < 0.01$ vs. CT.

Table 1.PROTACs and *t*-TUCB structures and inhibitory potency against sEH.

Compound	Structure	Human sEH IC ₅₀ nM ^a	Murine sEH IC ₅₀ nM ^a
<i>t</i> -TUCB		0.4	3.6
ALT-PG2		0.4	2.5
ALT-PG3		0.4	0.4

Author Manuscript

Author Manuscript

Author Manuscript

Author Manuscript